Critical percolation clusters in seven dimensions and on a complete graph

Wei Huang,[1] Pengcheng Hou,[1] Junfeng Wang,[2,*] Robert M. Ziff,[3,†] and Youjin Deng[1,4,‡]

[1]*Hefei National Laboratory for Physical Sciences at the Microscale and Department of Modern Physics, University of Science and Technology of China, Hefei, Anhui 230026, China*

[2]*School of Electronic Science and Applied Physics, Hefei University of Technology, Hefei, Anhui 230009, China*

[3]*Department of Chemical Engineering, University of Michigan, Ann Arbor, Michigan 48109-2136, USA*

[4]*CAS Center for Excellence and Synergetic Innovation Center in Quantum Information and Quantum Physics, University of Science and Technology of China, Hefei, Anhui 230026, China*

(Received 14 June 2017; revised manuscript received 19 December 2017; published 7 February 2018)

We study critical bond percolation on a seven-dimensional hypercubic lattice with periodic boundary conditions (7D) and on the complete graph (CG) of finite volume (number of vertices) V. We numerically confirm that for both cases, the critical number density $n(s,V)$ of clusters of size s obeys a scaling form $n(s,V) \sim s^{-\tau}\tilde{n}(s/V^{d_f^*})$ with identical volume fractal dimension $d_f^* = 2/3$ and exponent $\tau = 1 + 1/d_f^* = 5/2$. We then classify occupied bonds into *bridge* bonds, which includes *branch* and *junction* bonds, and *nonbridge* bonds; a bridge bond is a branch bond if and only if its deletion produces at least one tree. Deleting branch bonds from percolation configurations produces *leaf-free* configurations, whereas deleting all bridge bonds leads to *bridge-free* configurations composed of blobs. It is shown that the fraction of nonbridge (biconnected) bonds vanishes, $\rho_{n,CG} \to 0$, for large CGs, but converges to a finite value, $\rho_{n,7D} = 0.006\,193\,1(7)$, for the 7D hypercube. Further, we observe that while the bridge-free dimension $d_{bf}^* = 1/3$ holds for both the CG and 7D cases, the volume fractal dimensions of the leaf-free clusters are different: $d_{lf,7D}^* = 0.669(9) \approx 2/3$ and $d_{lf,CG}^* = 0.3337(17) \approx 1/3$. On the CG and in 7D, the whole, leaf-free, and bridge-free clusters all have the shortest-path volume fractal dimension $d_{min}^* \approx 1/3$, characterizing their graph diameters. We also study the behavior of the number and the size distribution of leaf-free and bridge-free clusters. For the number of clusters, we numerically find the number of leaf-free and bridge-free clusters on the CG scale as $\sim \ln V$, while for 7D they scale as $\sim V$. For the size distribution, we find the behavior on the CG is governed by a modified Fisher exponent $\tau' = 1$, while for leaf-free clusters in 7D, it is governed by Fisher exponent $\tau = 5/2$. The size distribution of bridge-free clusters in 7D displays two-scaling behavior with exponents $\tau = 4$ and $\tau' = 1$. The probability distribution $P(C_1,V)dC_1$ of the largest cluster of size C_1 for whole percolation configurations is observed to follow a single-variable function $\overline{P}(x)dx$, with $x \equiv C_1/V^{d_f^*}$ for both CG and 7D. Up to a rescaling factor for the variable x, the probability functions for CG and 7D collapse on top of each other within the entire range of x. The analytical expressions in the $x \to 0$ and $x \to \infty$ limits are further confirmed. Our work demonstrates that the geometric structure of high-dimensional percolation clusters cannot be fully accounted for by their complete-graph counterparts.

DOI: 10.1103/PhysRevE.97.022107

I. INTRODUCTION

At the threshold p_c, the percolation process leads to random, scale-invariant geometries that have become paradigmatic in theoretical physics and probability theory [1–4]. In two dimensions, a host of exact results are available. The bulk critical exponents $\beta = 5/36$ (for the order parameter) and $\nu = 4/3$ (for the correlation length) are predicted by Coulomb-gas arguments [5], conformal field theory [6], and stochastic Loewner evolution (SLE) theory [7], and are rigorously confirmed in the specific case of triangular-lattice site percolation [8]. In high dimensions, above the upper critical dimensionality $d_u = 6$, the mean-field values $\beta = 1$ and $\nu = 1/2$ are believed to hold [9–11]. For dimensions $2 < d < d_u$, exact values of exponents are unavailable, and the estimates of β and ν depend primarily upon numerical simulations [12–14].

Two simple types of lattices or graphs have been used to model infinite-dimensional systems: the Bethe lattice (or Cayley tree) and the complete graph (CG). A Bethe lattice is a tree on which each site has a constant number z of branches, and the percolation process becomes a branching process with threshold $p_c = 1/(z-1)$ [1]. On a finite CG of V sites, there exist $V(V-1)/2$ links between all pairs of sites; the bond probability is denoted as p with $p_c = 1/(V-1)$ [15,16]. In the thermodynamic limit of $V \to \infty$, bond percolation on the Bethe lattice and the CG both lead to the critical exponents $\beta = 1$ and $\nu = 1/2$. In this limit, the CG becomes essentially the Bethe lattice because the probability of forming a loop vanishes. In this paper, we compare and contrast periodic seven-dimensional (7D) lattice percolation with the CG for large but finite systems. The Bethe lattice would not be a good system to compare with because, for a finite system, it has a large boundary and many nonisotropic sites.

*wangjf@hfut.edu.cn
†rziff@umich.edu
‡yjdeng@ustc.edu.cn

In the Monte Carlo study of critical phenomena, finite-size scaling (FSS) provides a key computational tool for estimating critical exponents. Consider bond percolation on a d-dimensional lattice with linear size L, in which each link of a lattice is occupied with probability p. FSS predicts that near the percolation threshold p_c, the largest-cluster size C_1 scales asymptotically as

$$C_1(t,L) = L^{d_f}\tilde{C}_1(tL^{y_t}) \quad (t = p - p_c), \tag{1}$$

where the thermal and magnetic exponents, y_t and d_f, are related to the bulk exponents as $y_t = 1/\nu$ and $d - d_f = \beta/\nu$, and $\tilde{C}_1$ is a universal function, if we include system-dependent metric factors in its argument and coefficient. The exponent d_f is the standard fractal dimension of the clusters.

Although well established for $d < d_u$, FSS for $d > d_u$ is surprisingly subtle and depends significantly on the boundary conditions [17]. For instance, near and at the percolation threshold p_c, it is predicted that the thermal exponent for the correlation length and the fractal dimension are $(y_t,d_f) = (2,4)$ [18] for systems with free boundary conditions, and they are $(d/3,2d/3)$ [19] for systems with periodic boundary conditions. At p_c, the largest cluster size on the CG scales as $C_1 \propto V^{2/3}$, implying a volume fractal dimension $d_f^* = 2/3$ [20]. The volume thermal exponent for the CG is also known to be $y_t^* = 1/3$ [2]. An interesting question arises: how well does the CG describe other aspects of high-dimensional percolation for $d > d_u$?

In this work, we simulate bond percolation on the 7D hypercubic lattice with periodic boundary conditions and on the CG. We confirm the FSS of the size of the largest critical cluster $C_1 \propto V^{2/3}$ for both systems. Furthermore, we show that the cluster number $n(s,V)$ of size s per site at p_c obeys a universal scaling form,

$$n(s,V) = n_0 s^{-\tau}\tilde{n}(s/V^{d_f^*}), \quad \tilde{n}(x \to 0) = 1, \tag{2}$$

where $d_f^* = 2/3$ is a volume fractal dimension, equal to d_f/d for spatial systems, exponent $\tau = 1 + 1/d_f^* = 5/2$, n_0 is a nonuniversal constant, and $\tilde{n}$ is a universal function, if we include metric factors in their arguments. We numerically confirm that n_0 for the CG is equal to $(2\pi)^{-1/2} \approx 0.3989$ [21], while for 7D, $n_0 = 0.527(7)$, which is definitely higher than $(2\pi)^{-1/2}$. The probability distribution $P(C_1,V)dC_1$ of the largest cluster of size C_1 is observed to follow a single-variable function $\overline{P}(x)dx$ with $x \equiv C_1/V^{d_f^*}$, consistent with the theoretical results on the CG [22–24] and on sufficiently high-dimensional tori in Refs. [25–28]. In addition, we verify the limiting analytical forms of $\overline{P}(x)$ for $x \to 0$ and $x \to \infty$, derived for CG [23] and conjectured for 7D [28].

We then consider a natural classification of the occupied bonds of a percolation configuration and study the FSS of the resulting clusters, following the procedure in Ref. [29]. The occupied bonds are divided into *bridge* bonds and *nonbridge* bonds, and bridge bonds are further classified as *branch* bonds and *junction* bonds. A bridge bond is an occupied bond whose deletion would break a cluster into two. The bridge bond is a junction bond if neither of the two resulting clusters is a tree; otherwise, it is a branch bond. Deleting all branch bonds from percolation configurations leads to *leaf-free* configurations, which have no trees, and further deleting junctions produces *bridge-free* configurations. This process is shown schematically in Fig. 1. Other terminology is to call leaves and trees "dangling ends" and the bridge-free clusters "biconnected" or "blobs." The junction bonds are called "red bonds" when they are along the conduction path of the system, and in general not all junction bonds are red bonds. In combinatorics, the leaf-free configuration is called the 2-core of the whole percolation configuration [30].

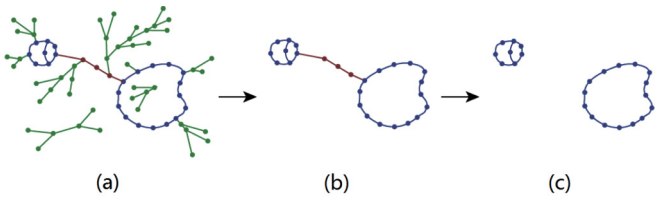

FIG. 1. Sketch of the types of bonds and clusters considered here: (a) the whole percolation clusters, (b) leaf-free clusters in which all trees composed of branch bonds (green) have been removed, including the removal of entire clusters if they are completely trees, and (c) bridge-free clusters or blobs (blue), in which all junction bonds (brown) as well as branch bonds have been removed.

We find that while the fraction of nonbridge bonds vanishes, $\rho_{n,CG}(V \to \infty) = 0$, for infinitely large CGs at criticality, it converges to a finite thermodynamic value $\rho_{n,7D} = 0.006\,193\,1(7)$ for 7D percolation. This implies that in contrast to the complete-graph case, the number of loops or blobs in finite-d critical percolation configurations is proportional to volume, $V = L^d$. We further determine the volume fractal dimensions of the leaf-free and bridge-free clusters as $d_{lf,7D}^* = 0.669(9) \approx 2/3$ and $d_{bf,7D}^* = 0.332(7) \approx 1/3$ for 7D, and $d_{lf,CG}^* = 0.3337(17) \approx 1/3$ and $d_{bf,CG}^* = 0.3337(15) \approx 1/3$ on the CG. While the bridge-free clusters apparently share the same fractal dimension, $d_{bf}^* = 1/3$, for the two systems, the leaf-free clusters have dramatically different fractal dimensions and scaling exponents. We also determine the shortest-path volume fractal dimension d_{min}^*, characterizing the graph diameters of clusters [27,31,32], and find that they are $d_{min,CG}^* = d_{min,7D}^* \approx 1/3$ for all the whole, leaf-free, and bridge-free clusters.

Moreover, we confirm that the number of leaf-free and bridge-free clusters on the CG is proportional to $\ln V$, while we find they are proportional to V in 7D. Further, we find the behavior of the size distribution of leaf-free and bridge-free clusters on the CG is governed by a modified Fisher exponent, $\tau' = 1$, instead of the standard one, $\tau = 1 + 1/d_{lf}^* = 1 + 1/d_{bf}^* = 4$, which is related to the fact that the number of clusters is proportional to $\ln V$, while the distribution for leaf-free clusters in 7D is governed by Fisher exponent $\tau = 5/2$. However, the size distribution of bridge-free clusters in 7D displays two-scaling behavior with standard and modified Fisher exponents $\tau = 4$ and $\tau' = 1$, respectively.

The remainder of this paper is organized as follows. Section II describes the simulation algorithm and sampled quantities. In Sec. III, the Monte Carlo data are analyzed and results for bond densities, various fractal dimensions, number of clusters, as well as the size distribution $n(s,V)$ are presented. A discussion of these results is given in Sec. IV.

II. SIMULATION

A. Model

We study critical bond percolation on the 7D hypercubic lattice with periodic boundary conditions and on the CG, at their thresholds $p_c = 0.0786752(3)$ [33] and $zp_c = 1$ with the coordination number $z = V - 1$ [34], respectively. At the first step of the simulation, we produce the configurations of the percolation clusters. On the basis of these clusters, all occupied bonds are classified into three types: branch, junction, and nonbridge. Definitions of these terminologies have been given in Ref. [29] for two-dimensional percolation, and can be transplanted intact into the present models. A *leaf* is defined as a site which is adjacent to precisely one occupied bond, and a "leaf-free" configuration is then defined as a configuration without any leaves. In actual implementation, we generate the *leaf-free* configuration via the following iterative procedure, often referred to as *burning*. For each leaf, we delete its adjacent bond. If this procedure generates new leaves, we repeat it until no leaves remain. The bonds which are deleted during this iterative process are precisely the branch bonds, and the remaining bridge bonds in the leaf-free configurations are the junction bonds. If we further delete all junction bonds from the leaf-free configurations, then we obtain the bridge-free configurations. We note that the procedure of identifying the nonbridge bonds from a leaf-free configuration can be time consuming since it involves the check of global connectivity. In Sec. II B, we describe the algorithm we used to carry this out efficiently.

We simulated multiple system sizes for each model. For 7D lattice percolation, we simulated the linear system sizes $L = 5, 6, 7, 8, 9, 10, 11, 12, 14$ with no less than 10^6 independent samples for each L. For the CG, we simulated volumes $V = 2^8, 2^9, 2^{10}, ..., 2^{20}$ number of sites, generating at least 10^7 independent samples for each V.

B. Algorithm

Unlike in the planar case [29], we cannot take advantage of the associated loop configurations, so the algorithm for 2D is not suitable for percolation clusters in higher dimensions or on the CGs. To identify nonbridge bonds within leaf-free clusters, we developed an algorithm based upon a breadth-first growth algorithm, which could be seen as a special case of the matching algorithm [35,36]. Different from Ref. [36] in which loops between two points far apart have to be identified dynamically, we just need to identify all the loops within a cluster, which results in a simpler version of the algorithm.

Consider an arbitrary graph $G = (V, E)$ of V sites (vertices) labeled as $i = 1, \ldots, V$ connected by a set of $|E|$ edges. Similarly to the matching algorithm, we implement a directed graph G^* as an auxiliary representation of the system to identify loops within a leaf-free cluster. To represent the directed graph G^*, we set an array called $\mathcal{D}$ of size V; if a site j points to another site i, then we assign $\mathcal{D}(j) = i$.

Starting from a leaf-free cluster, we perform a breadth-first search from site i_0, and assign $\mathcal{D}(i_0) = i_0$. We add one edge at one step of the search to the site i_1 and assign $\mathcal{D}(i_1) = i_0$. Before adding a new edge to graph G^*, we check whether the new site i_n on the growth process has been visited before; if it has, then the new edge will close a loop. Once a loop forms at i_n, we follow the arrows backwards until the two backtracking paths meet. In this way, all the edges of the loop are identified. After identifying all the nonbridge bonds on the loop, we assign the value of the starting point of the loop to all the elements of G^* that belong to the loop. Once all the edges in a loop have been identified, we continue to perform breadth-first growth on the leaf-free cluster and identify all the remaining nonbridge bonds.

For critical percolation on the CGs, the percolation threshold p_c equals $1/(V-1)$, and thus p_c becomes small as V becomes large. Therefore, at the critical probability, most of the edges are unoccupied, and storing the occupied edges instead of all the edges in the system saves a large amount of computer memory.

The small p_c for both 7D and CG implies that many random numbers and many operations would be needed if all the potentially occupied edges were visited to decide whether or not they are occupied. The simulation efficiency would drop quickly as the coordination number increases. In our algorithm, we follow a more efficient procedure [37,38]. We define $P(i) \equiv (1 - p_c)^{i-1} p_c$ to be the probability that the first $(i-1)$ edges are empty (unoccupied) while the ith edge is occupied. The cumulative probability distribution $F(i)$ is then

$$F(i) = \sum_{i'=1}^{i} P(i') = 1 - (1 - p_c)^i, \tag{3}$$

which gives the probability that the number of bonds to the first occupied edge is less than or equal to i.

Now, supposing the current occupied edge is the i_0th edge, one can obtain the next-to-be occupied edge as the $(i_0 + i)$th edge by drawing a uniformly distributed random number $0 \leqslant r < 1$ and determining the value of i such that

$$F(i-1) \leqslant r < F(i). \tag{4}$$

Solving Eq. (4), we get

$$i = 1 + \lfloor \ln(r)/\ln(1 - p_c) \rfloor. \tag{5}$$

Thus, instead of visiting all the potentially occupied edges, we directly jump to the next-to-be occupied edge in the system, skipping all the unoccupied ones sequentially. This process is repeated until the state of all edges in the system have been decided. By this method, the simulation efficiency is significantly improved for small p_c. This procedure is especially beneficial for the CG, where the total number of bonds $V(V-1)/2$ can be huge.

C. Measured quantities

We measured the following observables in our simulations:

(1) The mean branch-bond density $\rho_b := N_b/(|E|p_c)$, where N_b is the number of branch bonds and $|E|$ is the total number of edges. Analogously, the mean junction-bond density ρ_j and the mean nonbridge-bond density ρ_n. It is clear that $\rho_b + \rho_j + \rho_n = 1$.

(2) The mean number N of whole percolation clusters, N_{lf} of the leaf-free clusters, and N_{bf} of the bridge-free clusters. Note that while an isolated site is counted as a whole percolation

cluster, it is burned out by definition and is not counted as a leaf-free or bridge-free cluster.

(3) The number density $n(s)$ of clusters of size s for the whole percolation clusters, $n_{\rm lf}(s)$ for the leaf-free clusters, and $n_{\rm bf}(s)$ for the bridge-free clusters.

(4) The size $\mathcal{C}_1$ of the largest whole percolation cluster. The mean size $C = \langle \mathcal{C}_1 \rangle$ of the largest whole percolation cluster, $C_{\rm lf}$ of the largest leaf-free cluster, and $C_{\rm bf}$ of the largest bridge-free cluster.

(5) The maximum "time" step $\mathcal{S}$ in the breadth-first growing procedure of each cluster is recorded, which is equal to the shortest-path length between the seed site and another site in the cluster. The length $\mathcal{S}$ is also called the chemical distance [31] and is proportional to the graph diameter [27,32]. The largest length $\mathcal{S}_1$ over all the critical clusters behaves as $S = \langle \mathcal{S}_1 \rangle \propto V^{d^*_{\rm min}}$ and is used to determine the shortest-path volume fractal dimension $d^*_{\rm min}$.

In addition, we measured the cluster number $n(s,V)$ of size s per site for all the whole, leaf-free, and bridge-free configurations, and the probability distribution $P(C_1,V)dC_1$ for the largest whole percolation cluster of size C_1.

TABLE I. Fit results for branch-bond density $\rho_{\rm b}$, junction-bond density $\rho_{\rm j}$, and nonbridge-bond density $\rho_{\rm n}$ on the CG and in 7D.

	ρ	ρ_0	y	a_0	$V_{\rm min}$	DF/χ^2
CG	$\rho_{\rm b}$	1.000 000(1)	0.667(2)	−2.01(4)	2^9	7/5
		0.999 999(1)	0.669(3)	−2.06(7)	2^{10}	6/4
		0.999 999(2)	0.669(4)	−2.05(12)	2^{11}	5/4
	$\rho_{\rm j}$	−0.000 000 1(1)	0.661(1)	0.151(2)	2^9	7/9
		−0.000 000 1(1)	0.662(2)	0.154(4)	2^{10}	6/8
		−0.000 000 1(1)	0.660(3)	0.150(7)	2^{11}	5/7
	$\rho_{\rm n}$	0.000 000 0(2)	0.666 8(5)	1.83(1)	2^9	7/11
		0.000 000 0(3)	0.666 6(8)	1.83(2)	2^{10}	6/10
		0.000 000 4(4)	0.665 1(12)	1.79(3)	2^{11}	5/8
7D	$\rho_{\rm b}$	0.985 330 2(2)	2/3	−0.017(12)	7^7	3/5
		0.985 330 5(3)	2/3	−0.038(23)	8^7	2/4
	$\rho_{\rm j}$	0.008 476 4(2)	0.661(2)	1.53(7)	6^7	3/2
		0.008 476 5(3)	0.664(8)	1.60(19)	7^7	2/2
	$\rho_{\rm n}$	0.006 193 1(3)	0.671(4)	−1.77(10)	6^7	3/1
		0.006 193 1(5)	0.671(11)	−1.75(29)	7^7	2/1

III. RESULTS

A. Bond densities

In the definition of bond densities ρ_i, the number of bonds is not only divided by $|E|$, but also by p_c, so they represent the fraction of each kind of bond, and $\rho_{\rm b} + \rho_{\rm j} + \rho_{\rm n} = 1$. We fit our Monte Carlo data for the densities $\rho_{\rm j}$, $\rho_{\rm b}$, and $\rho_{\rm n}$ to the finite-size scaling ansatz

$$\rho = \rho_0 + V^{-y}(a_0 + a_1 V^{-y_1} + a_2 V^{-y_2}), \tag{6}$$

where ρ_0 is the critical value of bond density in the thermodynamic limit, y is the leading correction exponent, and y_j ($j = 1,2$) are subleading exponents.

As a precaution against correction-to-scaling terms that we fail to include in the fitting ansatz, we impose a lower cutoff $L > L_{\rm min}$ on the data points admitted in the fit, and we systematically study the effect on the χ^2 value of increasing $L_{\rm min}$. Generally, the preferred fit for any given ansatz corresponds to the smallest $L_{\rm min}$ for which the goodness of fit is reasonable and for which subsequent increases in $L_{\rm min}$ do not cause the χ^2 value to drop by vastly more than one unit per degree of freedom. In practice, by "reasonable" we mean that $\chi^2/{\rm DF} \lessapprox 1$, where DF is the number of degrees of freedom.

In the fits for the CG data, we tried various values for y_1 and y_2 terms, and found fixing $y_1 = 1/3$ and $y_2 = 2/3$ lead to the most stable fitting results. Leaving y free in the fits of $\rho_{\rm b}$, $\rho_{\rm j}$, and $\rho_{\rm n}$ on the CG, we estimate $y = 0.669(6), 0.661(6), 0.666(3)$, respectively, which are all consistent with 2/3.

From the fits, we estimate for the CG that $\rho_{\rm b,0} = 0.999\,999(3) \approx 1$, $\rho_{\rm j,0} = -0.000\,000\,1(2) \approx 0$, and $\rho_{\rm n,0} = 0.000\,000\,3(7) \approx 0$. We note that $\rho_{\rm b,0} + \rho_{\rm j,0} + \rho_{\rm n,0} = 1$ within error bars, as expected. As the system tends to infinity, we conclude that $\rho_{\rm b,0}$ equals 1, while $\rho_{\rm j,0}$ and $\rho_{\rm n,0}$ are equal to 0, which agrees with the findings in Ref. [15]. This conclusion is consistent with the scenario for percolation on the Bethe lattice (Cayley tree) where all of the bonds are branches. Besides, we estimate a_0 for $\rho_{\rm b}$, $\rho_{\rm j}$, and $\rho_{\rm n}$ on the CG as $-2.05(18), 0.150(11), 1.80(7)$, respectively. We note that the sum of these values is equal to 0 within error bars, as expected.

For bond densities in 7D, we fixed $a_2 = 0$ and tried various values for y_1, and finally fixed $y_1 = 1$. Leaving y free in the fits of $\rho_{\rm j}$ and $\rho_{\rm n}$, we obtain $y = 0.664(12)$ and $0.671(17)$, respectively, which are consistent with 2/3. On this basis, we conjecture that the bond densities of various types in both systems are energy-density-like, for which the leading finite-size dependence is governed by the thermal exponent, $y_t^* - d = -2/3$. We note that this feature also holds for $d < d_{\rm u}$ [29,39].

For $\rho_{\rm b}$ in 7D, by contrast, we were unable to obtain stable fits with y free. Fixing $y = 2/3$, the resulting fits produce estimates of a that are consistent with zero. In fact, we find $\rho_{\rm b}$ is consistent with 0.985 330 for all $V \geqslant 10^7$ ($L \geqslant 10$). From the fits, we estimate densities of $\rho_{\rm b,0} = 0.985\,330\,4(6)$, $\rho_{\rm j,0} = 0.008\,476\,5(5)$, and $\rho_{\rm n,0} = 0.006\,193\,1(7)$. It is clear that the density of nonbridge bonds in 7D is not zero in the thermodynamic limit, but a finite value despite being rather small. Actually, this is an obvious fact since an elementary square face has a probability p^4 to form a small loop of four occupied bonds. From the Pattern theorem [40], one can further argue that the number of loops in a cluster is proportional to its size.

We note that $\rho_{\rm b,0} + \rho_{\rm j,0} + \rho_{\rm n,0} = 1$ within error bars. We also note that the estimates of a_0 for $\rho_{\rm j}$ and $\rho_{\rm n}$ are equal in magnitude and opposite in sign, which is as expected given that a_0 for $\rho_{\rm b}$ is consistent with zero. The fit details are summarized in Table I.

In Fig. 2, we plot $\rho_{\rm b}$, $\rho_{\rm j}$, and $\rho_{\rm n}$ of CG and 7D vs $V^{-2/3}$. For the CG, the plot clearly demonstrates that the leading finite-size corrections for $\rho_{\rm b}$, $\rho_{\rm j}$, and $\rho_{\rm n}$ are governed by exponent $-2/3$, and $\rho_{\rm b}$ tends to 1 while $\rho_{\rm j}, \rho_{\rm n}$ tend to 0 when the system tends to infinity. For 7D, the plot clearly demonstrates that the leading finite-size corrections for $\rho_{\rm j}$ and $\rho_{\rm n}$ are governed by exponent $-2/3$, while essentially no finite-size dependence can be discerned for $\rho_{\rm b}$.

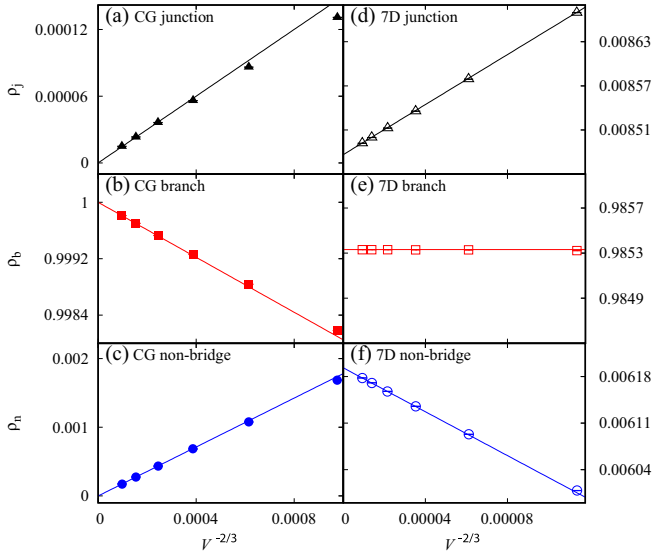

FIG. 2. (a),(d) Junction-bond densities ρ_j, (b),(e) branch-bond density ρ_b, and (c),(f) nonbridge-bond density ρ_n vs $V^{-2/3}$ on the CG (left) and in 7D (right). For the CG, from top to bottom, the intercept, respectively, corresponds to values 0,1,0. For 7D, from top to bottom, the three intercepts, respectively, correspond to values 0.008 476 5, 0.985 330 4, and 0.006 193 1. The statistical error of each data point is smaller than the symbol size. The straight lines are drawn simply to guide the eye.

B. Fractal dimensions

1. Fractal dimensions of clusters

In this section, we estimate the volume fractal dimensions d_f^*, d_{lf}^*, and d_{bf}^* from the observables C, C_{lf}, and C_{bf}, respectively, which are fitted to the finite-size scaling ansatz

$$\mathcal{O} = c_0 + V^{d_{\mathcal{O}}^*}(a_0 + a_1 V^{-y_1} + a_2 V^{-y_2} + a_3 V^{-y_3}), \qquad (7)$$

where $d_{\mathcal{O}}^*$ denotes the appropriate volume fractal dimension. The fit results are reported in Table II. In the reported fits, we set $c_0 = 0$ identically since leaving it free produced estimates for it consistent with zero.

For percolation on the CG, we fix $y_1 = 1/3$, $y_2 = 2/3$, and $y_3 = 1$. We estimate $d_f^* = 0.666\,4(5)$, which is consistent with the predicted volume fractal dimension of percolation clusters, $d_f^* = 2/3$. In addition, we estimate $d_{lf}^* = 0.333\,7(17)$ and $d_{bf}^* = 0.333\,7(15)$. In Fig. 3(a), we plot C_{lf} and C_{bf} on the CG vs V. We conjecture that both volume fractal dimensions of C_{lf} and C_{bf} on the CG are equal to $1/3$.

For percolation in 7D, we fix $y_1 = 1/3$, $y_2 = 2/3$, and $a_3 = 0$. We estimate $d_f = 0.669(9)$, which is consistent with the volume fractal dimension of percolation clusters, $d_f^* = 2/3$. Furthermore, we estimate $d_{lf}^* = 0.669(9)$ and $d_{bf}^* = 0.332(7)$. In Fig. 3(b), we plot C_{lf} and C_{bf} of 7D vs V to illustrate our estimates for d_{lf}^* and d_{bf}^*. We conjecture that $d_{lf}^* = 2/3$ while $d_{bf}^* = 1/3$.

As our numerical analysis shows, d_f^* and d_{bf}^* are consistent with each other on the CG and in 7D, while d_{lf}^* is not consistent for the two systems.

TABLE II. Fit results for the size of the largest whole percolation cluster C, the size of the largest leaf-free cluster C_{lf}, and the size of the largest bridge-free cluster C_{bf}. Entries with 0 means the fitting parameters are fixed at zero.

	$\mathcal{O}$	$d_{\mathcal{O}}^*$	a_0	a_1	V_{min}	DF/χ^2
CG	C	0.666 5(1)	0.942(2)	−0.21(2)	2^8	8/5
		0.666 4(2)	0.943(3)	−0.22(4)	2^9	7/5
		0.666 4(3)	0.944(4)	−0.24(7)	2^{10}	6/5
	C_{lf}	0.333 1(3)	0.834(4)	−1.22(5)	2^8	8/14
		0.333 5(5)	0.830(6)	−1.14(8)	2^9	7/12
		0.333 8(7)	0.826(9)	−1.07(14)	2^{10}	6/11
	C_{bf}	0.333 2(3)	0.700(3)	−0.49(4)	2^8	8/12
		0.333 5(5)	0.697(5)	−0.44(7)	2^9	7/11
		0.333 8(7)	0.693(7)	−0.38(12)	2^{10}	6/10
7D	C	0.665(2)	1.17(5)	0	5^7	3/4
		0.669(6)	1.08(13)	0	6^7	2/3
	C_{lf}	0.665(2)	0.107(4)	0	5^7	3/4
		0.669(6)	0.098(12)	0	6^7	2/3
	C_{bf}	0.332(2)	1.01(3)	0	5^7	3/4
		0.332(5)	1.01(9)	0	6^7	2/4

2. Shortest-path fractal dimension

We also determine the shortest-path volume fractal dimension d_{min}^* from the observable S for the whole, leaf-free, and bridge-free clusters, according to Eq. (7), with $y_1 = 1/3$, $y_2 = 2/3$, and $y_3 = 1$. The results are shown in Table III and in Fig. 4. It is noted that the analytical value $d_{min}^* = 1/3$ has been proved for the whole percolation clusters on the CG [32].

For both the CG and 7D, the shortest-path volume fractal dimension $d_{min}^* = 1/3$ remains unchanged after the branch and the junction bonds are sequentially removed. In 7D, despite the fact that most (≈98.5%) of the occupied bonds are branch bonds, their deletion has little effect on the shortest path—i.e., the values of S and S_{lf} are asymptotically equal. This suggests

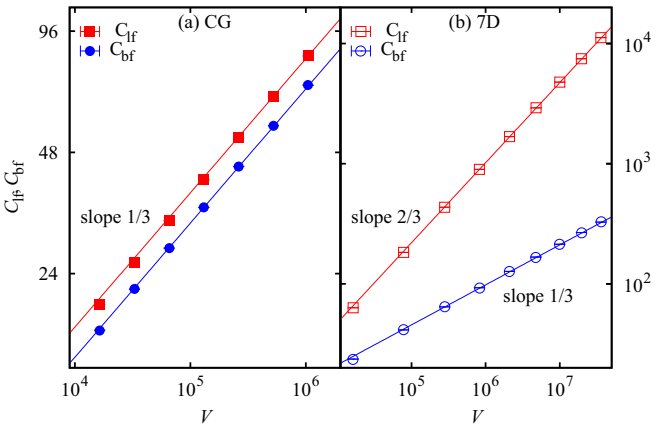

FIG. 3. (a) Log-log plot of C_{lf}, C_{bf} vs V on the CG. The two solid lines have slopes 1/3. The statistical error of each data point is smaller than the symbol size. The straight lines are simply to guide the eye. (b) Log-log plot of C_{lf}, C_{bf} vs V in 7D. The two solid lines have slopes 2/3 and 1/3, respectively. The statistical error of each data point is smaller than the symbol size. The straight lines are simply to guide the eye.

TABLE III. Fit results for the shortest path of the whole configurations S, of the leaf-free configurations $S_{\rm lf}$, and of the bridge-free configurations $S_{\rm bf}$. Entries with 0 means the fitting parameters are fixed at zero.

	S	$d^*_{\rm min}$	a_0	a_1	$V_{\rm min}$	DF/χ^2
CG	S	0.333 7(4)	2.33(2)	−3.4(3)	2^{12}	5/1
		0.333 5(7)	2.34(3)	−3.7(6)	2^{13}	4/1
		0.333 9(12)	2.32(4)	−3(1)	2^{14}	3/1
	$S_{\rm lf}$	0.333 1(5)	0.372(3)	−0.30(4)	2^{9}	8/2
		0.333 5(7)	0.370(4)	−0.26(7)	2^{10}	7/1
		0.333 4(11)	0.371(7)	−0.3(1)	2^{11}	6/1
	$S_{\rm bf}$	0.332 8(5)	0.311(2)	0	2^{9}	8/2
		0.333 1(7)	0.310(3)	0	2^{10}	7/1
		0.333 0(10)	0.310(3)	0	2^{11}	6/1
7D	S	0.334(2)	2.73(6)	−7(2)	6^{7}	3/1
		0.335(4)	2.7(2)	−5(7)	7^{7}	2/1
	$S_{\rm lf}$	0.334(2)	2.76(6)	−44(3)	6^{7}	3/1
		0.336(4)	2.7(2)	−37(9)	7^{7}	2/1
	$S_{\rm bf}$	0.330(3)	0.43(1)	0	7^{7}	3/4
		0.334(13)	0.39(7)	0	8^{7}	1/1

that the branch bonds in 7D form by themselves a huge number of small subcritical trees that have little impact on the geometric structure of clusters.

C. Number of clusters

According to [15], the average number of whole percolation clusters at criticality on the CG satisfies

$$N = V/2 + \mathrm{O}(\ln V). \tag{8}$$

The asymptotical cluster-number density $N/V \to 1/2$ can be qualitatively understood from Euler's formula $V = \mathcal{N} + \mathcal{B} - \mathcal{C}$ for an arbitrary graph, which relates the number of sites V, of clusters $\mathcal{N}$, of occupied bonds $\mathcal{B}$, and of cycles $\mathcal{C}$. For a finite CG at criticality, the average number of occupied bonds is $p_c|E| = (V-1)/2$ and the average density of cycles vanishes $\langle\mathcal{C}\rangle/V \to 0$ since all the occupied bonds are branch bonds for

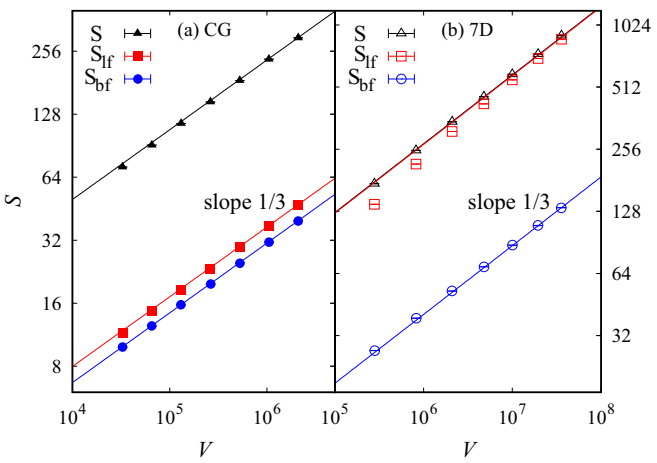

FIG. 4. Log-log plot of S, $S_{\rm lf}$, and $S_{\rm bf}$ vs V (a) on the CG and (b) in 7D. The solid lines have slopes 1/3. The statistical error of each data point is smaller than the symbol size.

TABLE IV. Fit results for the number of whole percolation clusters N, the number of leaf-free clusters $N_{\rm lf}$, and the number of bridge-free clusters $N_{\rm bf}$ on the CG and in 7D.

		a_0	a_1	$V_{\rm min}$	DF/χ^2
CG	N	0.500 000 1(1)	0.167(2)	2^{8}	14/9
		0.500 000 1(1)	0.166(4)	2^{9}	13/8
		0.500 000 1(2)	0.167(6)	2^{10}	12/7
	$N_{\rm lf}$	−0.487(4)	0.1665(2)	2^{8}	8/14
		−0.491(5)	0.1667(4)	2^{9}	7/13
		−0.503(9)	0.1675(6)	2^{10}	6/10
	$N_{\rm bf}$	−0.347(4)	0.1666(3)	2^{8}	8/12
		−0.351(6)	0.1668(4)	2^{9}	7/11
		−0.364(9)	0.1676(6)	2^{10}	6/9
7D	N	0.450 278 03(4)	1.36(8)	7^{7}	4/5
		0.450 278 06(5)	1.13(22)	8^{7}	3/4
	$N_{\rm lf}$	0.000 777 127(4)	1.01(4)	9^{7}	2/1
		0.000 777 130(6)	0.93(11)	10^{7}	1/1
	$N_{\rm bf}$	0.000 975 129(8)	−0.89(6)	8^{7}	2/3
		0.000 975 142(15)	−1.08(19)	9^{7}	1/1

$V \to \infty$. Thus, one has $\langle\mathcal{N}\rangle/V = 1 - \langle\mathcal{B}\rangle/V = 1/2$ in the thermodynamic limit. To verify Eq. (8), we study the number of whole percolation clusters at criticality on the CG and fit the data to the ansatz

$$N = a_0 V + a_1 \ln V + a_2 + a_3 V^{-1}. \tag{9}$$

The resulting fits are summarized in Table IV. Leaving a_3 free, we find that a_3 is consistent with zero, suggesting that the last subleading correction exponent in the ansatz might be even smaller than −1. We estimate $a_0 = 0.500\,000\,1(3) \approx 1/2$ and $a_1 = 0.167(9)$. In Fig. 5(a), we plot $\delta N := N - V/2$ vs V to illustrate the logarithmic correction of cluster number of critical percolation on the CG.

We also study the number of leaf-free clusters and bridge-free clusters on the CG. Since the fraction of the junction bonds and the nonbridge bonds, $\rho_{\rm j}$ and $\rho_{\rm n}$, vanishes as $\mathrm{O}(V^{-2/3})$, the number of isolated sites after burning is approaching V with a correction term $V^{-2/3}$. Note that in our definitions of leaf-free and bridge-free clusters, we do not include these isolated sites. As a result, the V term does not exist in $N_{\rm lf}$ or $N_{\rm bf}$. We find that $N_{\rm lf}$ and $N_{\rm bf}$ grow slowly as V tends to infinity. As suggested by [41], we fit the data to the ansatz

$$N_{\mathcal{O}} = a_0 + a_1 \ln V + a_2 V^{-1/3} + a_3 V^{-2/3} + a_4 V^{-1}, \tag{10}$$

where $N_{\mathcal{O}}$ represents $N_{\rm lf}$ or $N_{\rm bf}$. We estimate $a_0 = -497(22), -0.358(22)$ and $a_1 = 0.1672(9), 0.1673(10)$ for $N_{\rm lf}$ and $N_{\rm bf}$, respectively, which means that both the coefficient of the logarithmic term of the number N of leaf-free and of bridge-free clusters are consistent with the value 1/6. Combined with the results for N, this suggests that the logarithmic term in (8) comes from clusters containing cycles. We mention that in Ref. [21], they find that the average number of unicyclic components grows logarithmically with the system size as $\sim(1/6)\ln V$, which indicates that most leaf-free and bridge-free clusters are unicyclic components. In Fig. 5(b), we plot $N_{\rm lf}$ and $N_{\rm bf}$ vs V to illustrate the logarithmic growth of the number of leaf-free and bridge-free clusters.

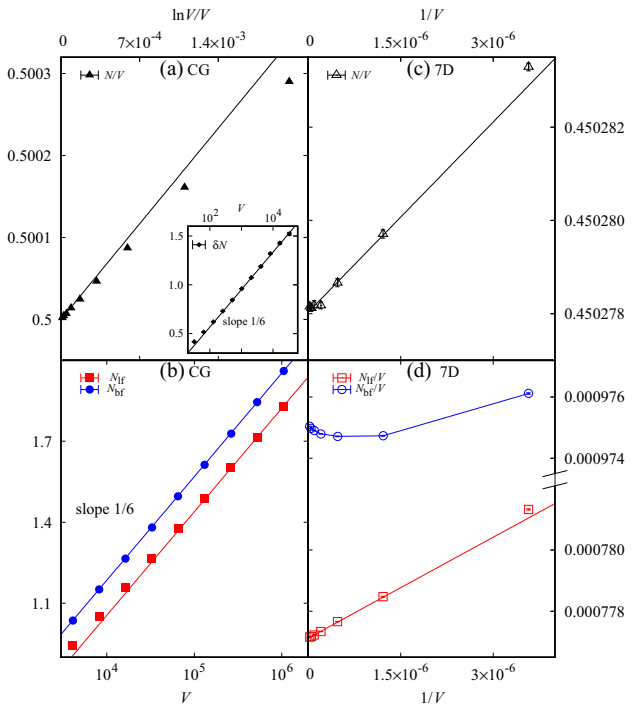

FIG. 5. (a) Plot of number density N/V of whole percolation clusters vs $(\ln V)/V$ on the CG. The inset is the semilogarithmic plot of δN vs V. (b) Semilogarithmic plot of total number $N_{\rm lf}$, $N_{\rm bf}$ of leaf-free and bridge-free clusters vs V on the CG. (c) Plot of the number density N/V of whole percolation clusters vs $1/V$ in 7D. (d) Plot of number density $N_{\rm lf}/V$, $N_{\rm bf}/V$ of leaf-free and bridge-free clusters vs $1/V$ in 7D.

For the 7D case, the behavior of cluster numbers is much different from the CG. We find that cluster-number densities of whole, leaf-free, and bridge-free clusters tend to a finite limit. This is demonstrated in Figs. 5(c) and 5(d). We find that the excess cluster number [42] could be found for whole percolation clusters and leaf-free clusters. For bridge-free clusters, however, the behavior is not linear, which implies that the excess cluster concept does not apply here. To estimate the excess cluster number of whole percolation clusters and leaf-free clusters, we fit the cluster number N and $N_{\rm lf}$ to the ansatz

$$N_{\mathcal{O}} = a_0 V + a_1, \tag{11}$$

where $N_{\mathcal{O}}$ represents N or $N_{\rm lf}$. We find that N and $N_{\rm lf}$ can be well fitted to the ansatz (11) and estimate the density of whole percolation clusters $a_0 = 0.450\,278\,06(9)$, the excess cluster number of whole percolation clusters $a_1 = 1.18(39)$, the density of leaf-free clusters $a_0 = 0.000\,777\,130(13)$, and the excess cluster number of leaf-free clusters $a_1 = 0.93(18)$. As illustrated by Fig. 5(d), the number density $N_{\rm bf}/V$ of bridge-free clusters does not scale monotonically as V increases. It will be shown later that for large size s, the cluster-size distribution $n_{\rm bf}(s,V)$ in 7D displays similar behavior as that on the CG; see Figs. 8(b)–8(d). Motivated by this observation, we conjecture that in addition to a term $\sim V$, the cluster number $N_{\rm bf}$ has a logarithmic term, $\sim \ln V$. On this basis, we fit the

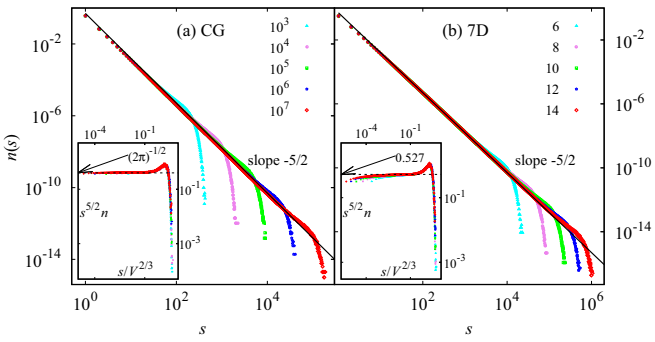

FIG. 6. Number density of whole percolation clusters of size s as a function of s (a) on the CG and (b) in 7D. The inset shows $n(s)s^{5/2}$ vs $s/V^{2/3}$ for the two systems.

$N_{\rm bf}$ data by the ansatz

$$N_{\rm bf} = a_0 V + a_1 \ln V + a_2, \tag{12}$$

and obtain the density of bridge-free clusters $a_0 = 0.000\,975\,139(27)$, $a_1 = -0.89(10)$, and $a_2 = 12(1)$.

D. Distribution

1. Cluster-size distribution

We also study the size distribution of the whole, leaf-free, and bridge-free clusters on the CG and in 7D.

For whole percolation configurations on the CG, Ref. [21] predicts that the critical number density $n(s,V)$ of clusters of size s follows a standard scaling form,

$$n(s,V) = n_0 s^{-\tau} \tilde{n}(s/V^{d_{\rm f}^*}) \quad [\tilde{n}(x \to 0) = 1], \tag{13}$$

with $n_0 = (2\pi)^{-1/2}$, volume fractal dimension $d_{\rm f}^* = 2/3$, and exponent $\tau = 1 + 1/d_{\rm f}^* = 5/2$. We numerically confirm this prediction as well as the value of n_0, as shown in Fig. 6(a). Further, it is predicted [21] that $n(s,V)$ has the following extremal behavior:

$$n(s,V) \simeq \exp[-(s/V^{d_{\rm f}^*})^{\gamma}], \quad s \gg V^{d_{\rm f}^*}, \tag{14}$$

with $\gamma = 3$ [23]. Similar scaling behavior of $n(s,V)$ is observed for whole percolation configurations in 7D, as shown in Fig. 6(b).

To quantitatively determine the metric factor n_0, we consider the total number N_t of clusters of size $V^{4/7} < s < 2V^{4/7}$, of which the finite-size scaling can be obtained by calculating the integral of Eq. (13) as

$$N_t = n_0 \frac{2\sqrt{2}-1}{3\sqrt{2}} V^{1/7}[1 + {\rm O}(V^{-y_2})]. \tag{15}$$

The leading exponent $1/7$ arises from the chosen range $(V^{4/7}, 2V^{4/7})$, which is to minimize the nonuniversal corrections from clusters of small sizes, $s = {\rm O}(1)$, and the cutoff effects from giant clusters of sizes $s = {\rm O}(V^{2/3})$, and the correction exponent is from the lattice effect. A V-dependent metric factor is defined as $n_{0,V} = 3\sqrt{2}N_t V^{-1/7}/(2\sqrt{2}-1)$, of which the Monte Carlo data are fitted by ansatz

$$n_{0,V} = n_0 + n_1 V^{-y_1} + n_2 V^{-y_2}, \tag{16}$$

TABLE V. Fit results of metric factor $n_{0,V}$ in Eq. (16) for the CG and 7D.

	n_0	y_1	$V_{\min}$	DF/χ^2
CG	0.3993(9)	1/7	2^{15}	5/4
	0.3990(10)	1/7	2^{16}	4/4
	$(2\pi)^{-1/2}$	0.142(2)	2^{15}	5/4
	$(2\pi)^{-1/2}$	0.144(4)	2^{16}	4/4
7D	0.525(2)	1/7	7^7	5/5
	0.528(4)	1/7	8^7	4/5

where $y_1 = 1/7$ and $y_2 = 4/7$. On the CG, we obtain $n_0 = 0.399(2) \approx (2\pi)^{-1/2} = 0.3989$; fixing $n_0 = (2\pi)^{-1/2}$ and $y_2 = 4/7$, we have $y_1 = 0.144(6) \approx 1/7$. For 7D, we find $n_0 = 0.527(7) > (2\pi)^{-1/2}$. The results are summarized in Table V and demonstrated in Fig. 7.

On the CG, the size distributions of leaf-free and bridge-free clusters, shown in Figs. 8(a) and 8(b), both have a modified Fisher exponent, $\tau' = 1$, instead of the standard one, $\tau = 1 + 1/d_{\rm lf}^* = 4$. From Figs. 8(a) and 8(b), we conjecture that the distribution $n(s,V)$ obeys

$$n(s,V) = n_0 s^{-\tau'} V^{-h} \tilde{n}(s/V^{d_{\mathcal{O}}^*}) \quad [\tilde{n}(x \to 0) = 1], \tag{17}$$

where $d_{\mathcal{O}}^* = 1/3$ is the volume fractal dimension. This leads to the total cluster number $n(V)$ per site as

$$\int n(s,V)ds \sim \begin{cases} \frac{n_0}{3}(\ln V)V^{-h} & \text{if } \tau' = 1, \\ \frac{n_0}{-\tau'+1} V^{\frac{1}{3}(-\tau'+1)-h} & \text{if } \tau' \neq 1. \end{cases} \tag{18}$$

From the known result $n(V) \approx (\ln V)/6V$ [21], one obtains $\tau' = 1$, $h = 1$, and $n_0 = 1/2$. The insets of Fig. 8(a) and 8(b) confirm the conjectured scaling function (17), including $n_0 = 1/2$. It can be seen that the anomalous behavior of the modified Fisher exponent τ' is due to the vanishing cluster-number density $n(V \to \infty) = 0$; this phenomenon has been already observed elsewhere [43].

In 7D, the cluster-size distribution of leaf-free clusters follows the standard form $n(s,V) \sim s^{-5/2}\tilde{n}(s/V^{2/3})$ [Fig. 8(c)]. Interestingly, for bridge-free clusters, $n(s,V)$ displays two-scaling behavior [Fig. 8(d)], which has a standard Fisher exponent $\tau = 1 + 1/d_{\rm bf}^* = 4$ for $s \ll V^{1/3}$ and a modified one $\tau' = 1$ for $s = \mathrm{O}(V^{1/3})$. The former arises from the extensivity

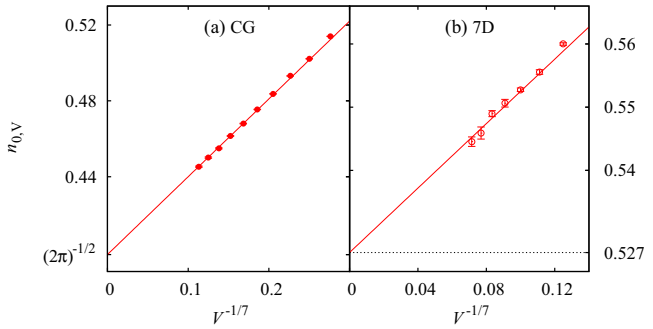

FIG. 7. Metric factor $n_{0,V}$ vs $V^{-1/7}$ (a) on the CG and (b) in 7D. The intercepts, respectively, correspond to the values $(2\pi)^{-1/2}$ and 0.527.

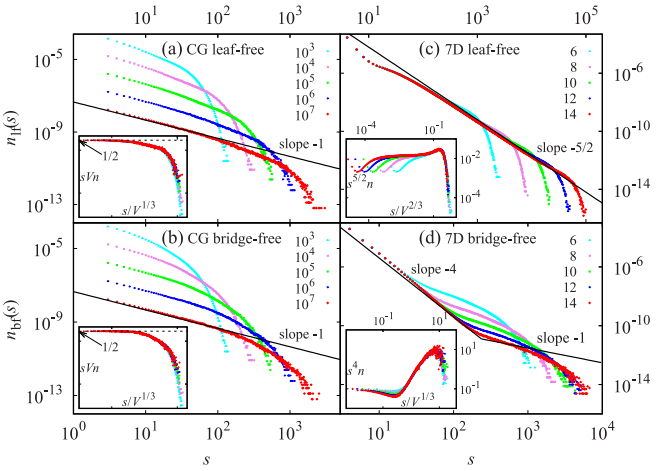

FIG. 8. Number density of (a) leaf-free clusters on the CG, (b) bridge-free clusters on the CG, (c) leaf-free clusters in 7D, and (d) bridge-free clusters in 7D of size s as a function of s. The inset shows (a) $sVn_{\rm lf}(s)$ vs $s/V^{1/3}$ on the CG, (b) $sVn_{\rm bf}(s)$ vs $s/V^{1/3}$ on the CG, (c) $n_{\rm lf}(s)s^{5/2}$ vs $s/V^{2/3}$ in 7D, and (d) $s^4 n_{\rm bf}(s)$ vs $s/V^{1/3}$ in 7D.

of clusters of small sizes, and the latter reflects the sparsity of giant clusters, as for the CG case.

2. *Size distribution of the largest cluster*

We study the probability distribution $P(C_1,V)dC_1$ of the largest whole percolation cluster. On the CG, Ref. [22] predicts that $P(C_1,V)dC_1$ can be expressed as a single-variable function $\overline{P}(x)dx$, with $x \equiv C_1/V^{d_{\rm f}^*}$ ($d_{\rm f}^* = 2/3$). The inset of Fig. 9 confirms this prediction for the CG and demonstrates that it also holds for 7D.

We further rescale the variable x by a constant factor a as $\tilde{x} = x/a$, so that one has $\tilde{P}(\tilde{x}) = a\overline{P}(a\tilde{x})$ from $\tilde{P}(\tilde{x})d\tilde{x} = \overline{P}(x)dx$. With $a_{\rm CG} = 1, a_{\rm 7D} \approx 1.2$, we observe that within the numerical uncertainty, the functions $\tilde{P}_{\rm CG}(\tilde{x})$ and $\tilde{P}_{\rm 7D}(\tilde{x})$ well

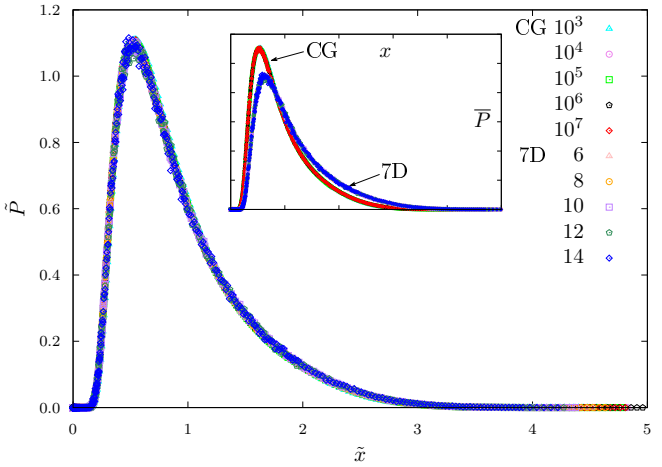

FIG. 9. Rescaled size distribution $\tilde{P}(\tilde{x})$ of the largest cluster vs $\tilde{x} \equiv (1/a)C_1/V^{2/3}$ on the CG and in 7D, with $(a_{\rm CG} = 1, a_{\rm 7D} = 1.2)$. The inset shows the nonrescaled probability function $\overline{P}(x)$ with $x \equiv C_1/V^{2/3}$.

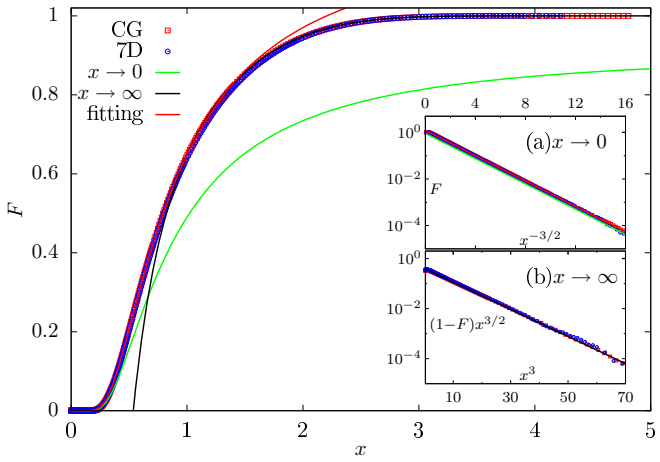

FIG. 10. Cumulative probability $F(x)$ on the CG ($V = 10^7$) and in 7D ($V = 14^7$). The green and black lines represent the analytical functions by Eq. (19), respectively, for $x \to 0$ and $x \to \infty$. The red line is also for Eq. (19), but with $b_0 = 1.21$ given by the fit. Insets (a) and (b) correspond to the theoretical predictions (19) for $x \to 0$ and $x \to \infty$, respectively.

collapse on top of each other over the entire range of $\tilde{x}$ (Fig. 9). Therefore, we conjecture that the finite-size distribution of the largest cluster for CG and $d \geqslant d_u$ follows a single-variable function, which is universal up to a nonuniversal factor.

We then consider the cumulative distribution $F(x) \equiv \int_0^x \tilde{P}(\tilde{x}')d\tilde{x}'$, which should be the same for the CG and 7D, as supported by Fig. 10. On the CG ($a_{\rm CG} = 1$), the extremal behaviors are proven in Ref. [23] and one has, at the critical point,

$$F(x) = \begin{cases} b_0 \exp(-b_1 x^{-3/2}) & \text{if } x \to 0, \\ 1 - c_0 x^{-3/2} \exp(-c_1 x^3) & \text{if } x \to \infty, \end{cases} \tag{19}$$

with b_0, b_1, c_0, and c_1 being definite-positive coefficients. In addition, it is derived on the CG [23] that the coefficients $c_0 = (2\pi)^{-1/2}$ and $c_1 = 1/8$, and the exact values of b_0 and b_1, can be obtained as

$$b_0 = (\gamma_e \pi)^{1/4} (\mu e^{-\mu})^{1/2} e^{\mu_0}, \quad b_1 = \frac{2e^{\mu}}{3\sqrt{2\pi}},$$
$$\mu_0 = (1/4) \int_0^{\mu} dt (e^t - 1)/t, \tag{20}$$

where $\gamma_e = \lim_{m\to\infty}(\sum_{j=1}^{m} 1/j - \ln m) \doteq 0.5772$ is the Euler's constant and $\mu \doteq 0.85403$ is the root of $\mu^{-1/2} e^{\mu} = \int_0^{\mu} t^{-1/2} e^t dt$. This gives $b_0 \doteq 0.916$ and $b_1 \doteq 0.6247$. Our conjecture predicts that the extremal behaviors for both CG and 7D would obey Eq. (19), consistent with a recent conjecture by Heydenreich and van der Hofstad [28]. The insets of Fig. 10 demonstrate that with $a_{\rm 7D} \approx 1.2$, they are indeed described by Eq. (19). By fitting the numerical data, we determine $c_0 = 0.41(1), c_1 = 0.125(1), b_0 = 1.21(2)$, and $b_1 = 0.6250(6)$. Except b_0, these estimates are in good agreement with their exact values. We show in Fig. 10 the analytical curves by Eq. (19) with the exact values of the coefficients, as well as the fitting curve with $b_0 = 1.21$. It is seen that the fitting curve describes the numerical data in a wider range of x than the analytical one. We also note that if the value of μ_0 in Eq. (20) were doubled, one would have $b_0 \doteq 1.199$, consistent with the numerical estimate $b_0 = 1.21(2)$.

IV. DISCUSSION

We have studied the geometric structure of critical bond percolation on the complete graph (CG) and on the 7D hypercubic lattice with periodic boundary conditions, by separating the occupied edges into three natural classes. We found that bridge-free clusters have the same volume fractal dimension (1/3) on the CG and in 7D, while leaf-free configurations do not (1/3 and 2/3, respectively). The shortest-path volume fractal dimension is consistent with 1/3 on the whole, leaf-free, and bridge-free configurations and for both the CG and 7D.

The study of three kinds of bond densities on the CG and in 7D provided more details about the geometric properties of percolation between the two models. Similar to the 2D case [29], the density of branches in 7D is only very weakly dependent on the system size, although they occupy around 98.5 percent of the occupied bonds in the system. On the other hand, the density of branch bonds on the CG tends to 1 in the thermodynamic limit. The different behaviors of density of branches between the CG and 7D may result in the difference of leaf-free cluster fractal dimensions between CG and 7D.

From our work, we obtain the following general picture of percolation on the CG and in 7D:

On the CG, in the limit of $V \to \infty$, the connectivity becomes identical to a Bethe lattice with an infinite number of possible bonds at each vertex, but with, on average, just one of those bonds being occupied at the critical point. The total number of blobs (bridge-free clusters) $N_{\rm bf}$ is nonextensive and increases logarithmically, instead of linearly, with the system size V. Figure 8 further demonstrates that for a given size $s \ll V^{d^*_{\rm bf}} = V^{1/3}$, the number of blobs $N(s)$ remains as a finite constant, which is inversely proportional to size s. As a consequence, one has a modified Fisher exponent, $\tau' = 1$, instead of the standard one, $\tau = 1 + 1/d^*_{\rm bf} = 4$. The giant clusters and the few blobs are what distinguishes the CG from the Bethe lattice, which is problematic here because of its large surface area. The critical exponents such as $\tau = 5/2$ are the same for the CG and the Bethe lattice, being the mean-field values, but other properties are different.

In 7D percolation, the critical exponents are also mean field, so in that sense the system is similar to the CG and Bethe lattice. The blobs in 7D do have the volume fractal dimension $d^*_{\rm bf} = 1/3$, the same as for the CG; however, they are much more numerous and represent a finite fraction of the clusters in the system. Still, on an overall scale, the collection of clusters has a tree structure, decorated with blobs in various places. The tree can have branch points where more than two junction bonds visit a single point or where more than two junction bonds connect to a blob. The branch bonds, despite constituting 98.5% of the total occupied bonds, form an extensive number of small subcritical trees with finite sizes. Deletion of these leaves barely changes the graph diameters of giant clusters, as suggested by Fig. 4. The scenario of treelike cluster structures decorated with blobs is well supported by the size distribution of the largest cluster, which is observed to follow the same universal and single-variable function as that for the CG.

Table VI summarizes the estimates presented in this work.

TABLE VI. Summary of estimated bond densities in the thermodynamic limit ρ_0 in Eq. (6), leading finite-size correction exponents for bond densities y in Eq. (6); volume fractal dimensions $d^*_{\mathcal{O}}$ in Eq. (7), volume fractal shortest-path dimensions $d^*_{\min}$ in Eq. (7), cluster-number density a_0 of whole percolation clusters in Eq. (9) on the CG, cluster-number density a_0 of whole percolation clusters, leaf-free clusters in Eq. (11) and bridge-free clusters in Eq. (12) in 7D, coefficient of logarithmic term a_1 of whole percolation clusters in Eq. (9), leaf-free and bridge-free clusters a_1 in Eq. (10) on the CG, and excess cluster number a_1 of whole percolation clusters and leaf-free clusters in Eq. (11) in 7D, and metric factor n_0 in Eq. (16).

	CG			7D		
	Branch bonds	Junction bonds	Nonbridge bonds	Branch bonds	Junction bonds	Nonbridge bonds
ρ_0	0.999999(3) ≈ 1	$-0.0000001(2) \approx 0$	$0.0000003(7) \approx 0$	0.985 330 4(6)	0.008 476 5(5)	0.006 193 1(7)
y	$0.669(6) \approx 2/3$	$0.661(6) \approx 2/3$	$0.666(3) \approx 2/3$		$0.664(12) \approx 2/3$	$0.671(17) \approx 2/3$
	Whole cluster	Leaf-free cluster	Bridge-free cluster	Whole cluster	Leaf-free cluster	Bridge-free cluster
$d^*_{\mathcal{O}}$	$0.6664(5) \approx 2/3$	$0.3337(17) \approx 1/3$	$0.3337(15) \approx 1/3$	$0.669(9) \approx 2/3$	$0.669(9) \approx 2/3$	$0.332(7) \approx 1/3$
$d^*_{\min}$	$0.3339(18) \approx 1/3$	$0.3334(15) \approx 1/3$	$0.3330(15) \approx 1/3$	$0.335(6) \approx 1/3$	$0.3338(24) \approx 1/3$	$0.334(18) \approx 1/3$
a_0	0.5000001(3) $\approx 1/2$			0.450 278 06(9)	0.000 777 130(13)	0.000 975 139(27)
a_1	$0.167(9) \approx 1/6$	$0.1672(9) \approx 1/6$	$0.1673(10) \approx 1/6$	1.18(39)	0.93(18)	
n_0	$0.3991(17) \approx (2\pi)^{-1/2}$	1/2	1/2	0.527(7)		

We compare these results with the 2D results [29], which is below the critical dimension 6, so universality holds. The general scenario for the geometric structure of critical percolation clusters is the same for all finite dimensions: the leaf-free clusters have the same fractal dimension as the whole percolation cluster, and the bridge-free clusters (blobs) have the dimension of backbone clusters. For $d \geqslant d_u$, the blobs are mostly unicycles, while the blobs in lower dimensions have many cycles. It would be of interest to check this scenario in more detail.

A natural question to ask is to what extent the results of percolation on a seven-dimensional lattice with periodic boundary carry over to that with free boundary conditions. It is argued [17] that although the largest clusters with free boundary conditions have fractal dimension $d_f = 4$ (independent of spatial dimension), at the pseudocritical point with free boundary conditions giant clusters can have fractal dimension $d_f = 2d/3$. Another generalization is to study the q-state random-cluster model, particularly $q = 2$ [44]. Since these arguments are by no means rigorous, it is important to carry out large-scale Monte Carlo simulations, although there will be difficulties due to the limitations on the size of the system that can be simulated.

ACKNOWLEDGMENTS

We acknowledge P. J. Zhu and Y. B. Zhang for their contributions in the initial stage of this project. We also thank Z. Z. Zhou for valuable discussions. This work was supported by the National Science Fund for Distinguished Young Scholars (NSFDYS) under Grant No. 11625522 (Y.J.D.), the National Natural Science Foundation of China (NSFC) under Grant No. 11405039 (J.F.W.), and the Fundamental Research Fund for the Central Universities under Grant No. J2014HGBZ0124 (J.F.W.). R.M.Z. thanks the USTC for the hospitality while this paper was written.

[1] D. Stauffer and A. Aharony, *Introduction To Percolation Theory*, 2nd ed. (Taylor & Francis, London, 1994).
[2] G. R. Grimmett, *Percolation*, 2nd ed. (Springer, Berlin, 1999).
[3] B. Bollobás and O. Riordan, *Percolation* (Cambridge University Press, Cambridge, 2006).
[4] N. A. M. Araújo, P. Grassberger, B. Kahng, K. J. Schrenk, and R. M. Ziff, Recent advances and open challenges in percolation, Europhys. J. Spec. Top. **223**, 2307 (2014).
[5] B. Nienhuis, in *Phase Transition and Critical Phenomena*, edited by C. Domb, M. Green, and J. L. Lebowitz (Academic, London, 1987), Vol. 11.
[6] J. L. Cardy, in *Phase Transition and Critical Phenomena*, edited by C. Domb, M. Green, and J. L. Lebowitz (Academic, London, 1987), Vol. 11.
[7] G. F. Lawler, O. Schramm, and W. Werner, The dimension of the planar Brownian frontier is 4/3, Math. Res. Lett. **8**, 401 (2001).
[8] S. Smirnov and W. Werner, Critical exponents for two-dimensional percolation, Math. Res. Lett. **8**, 729 (2001).
[9] A. Aharony, Y. Gefen, and A. Kapitulnik, Scaling at the percolation threshold above six dimension, J. Phys. A **17**, L197 (1984).
[10] T. Hara and G. Slade, Mean-field critical behavior for percolation in high dimensions, Commun. Math. Phys. **128**, 333 (1990).
[11] R. Fitzner and R. van der Hofstad, Mean-field behavior for nearest-neighbor percolation in $d > 10$, Electron. J. Prob. **22**, 1 (2017).
[12] J. F. Wang, Z. Z. Zhou, W. Zhang, T. M. Garoni, and Y. J. Deng, Bond and site percolation in three dimensions, Phys. Rev. E **87**, 052107 (2013).
[13] X. Xu, J. F. Wang, J. P. Lv, and Y. J. Deng, Simultaneous analysis of three-dimensional percolation models, Front. Phys. **9**, 113 (2014).
[14] G. Paul, R. M. Ziff, and H. E. Stanley, Percolation threshold, Fisher exponent, and shortest path exponent for four and five dimensions, Phys. Rev. E **64**, 026115 (2001).
[15] P. Erdős and A. Rényi, On the evolution of random graphs, Publ. Math. Inst. Hungar. Acad. Sci. **5**, 17 (1960).

[16] V. E. Stepanov, Phase transitions in random graphs, Theory Prob. Appl. **15**, 187 (1970).
[17] R. Kenna and B. Berche, Universal finite-size scaling for percolation theory in high dimensions, J. Phys. A **50**, 235001 (2017).
[18] T. Hara, Decay of correlations in nearest-neighbor self-avoiding walk, percolation, lattice trees and animals, Ann. Prob. **36**, 530 (2008).
[19] M. Heydenreich and R. van der Hofstad, Random graph asymptotics on high-dimensional tori, Comm. Math. Phys. **270**, 335 (2007).
[20] S. Janson, D. E. Knuth, T. Łuczak, and B. Pittel, The birth of the giant component, Random Struct. Alg. **4**, 71 (1993).
[21] E. Ben-Naim and P. L. Krapivsky, Kinetic theory of random graphs: From paths to cycles, Phys. Rev. E **71**, 026129 (2005).
[22] D. Aldous, Brownian excursions, critical random graphs and the multiplicative coalescent, Ann. Prob. **25**, 812 (1997).
[23] B. Pittel, On the largest component of the random graph at a near critical stage, J. Comb. Theory, Ser. B **82**, 237 (2001).
[24] R. van der Hofstad, W. Kager, and T. Muller, A local limit theorem for the critical random graph, Electron. Commun. Prob. **14**, 122 (2009).
[25] C. Borgs, J. T. Chayes, R. van der Hofstad, G. Slade, and J. Spencer, Random subgraphs of finite graphs: I. The scaling window under the triangle condition, Random Struc. Alg. **27**, 137 (2005).
[26] C. Borgs, J. T. Chayes, R. van der Hofstad, G. Slade, and J. Spencer, Random subgraphs of finite graphs: II. The lace expansion and the triangle condition, Ann. Prob. **33**, 1886 (2005).
[27] M. Heydenreich and R. van der Hofstad, Random graph asymptotics on high-dimensional tori II: Volume, diameter and mixing time, Prob. Theory Relat. Fields **149**, 397 (2011).
[28] M. Heydenreich and R. van der Hofstad, *Progress in High-Dimensional Percolation and Random Graphs* (Springer, Switzerland, 2017).
[29] X. Xu, J. F. Wang, Z. Z. Zhou, T. M. Garoni, and Y. J. Deng, Geometric structure of percolation clusters, Phys. Rev. E **89**, 012120 (2014).
[30] T. Łuczak, Size and connectivity of the k-core of a random graph, Discrete Math. **91**, 61 (1991).
[31] S. Havlin and R. Nossal, Topological properties of percolation clusters, J. Phys. A **17**, L427 (1984).
[32] A. Nachmias and Y. Peres, Critical random graphs: Diameter and mixing time, Ann. Prob. **36**, 1267 (2008).
[33] P. Grassberger, Critical percolation in high dimensions, Phys. Rev. E **67**, 036101 (2003).
[34] In the literature, the percolation threshold on the CG is sometimes taken as $p_c = 1/V$. The difference between $1/(V-1)$ and $1/V$ is $O(V^{-1})$, which is insignificant in comparison with the scaling window, $O(V^{-1/3})$.
[35] C. Moukarzel, An efficient algorithm for testing the generic rigidity of graphs in the plane, J. Phys. A **29**, 8079 (1996).
[36] C. Moukarzel, A fast algorithm for backbones, Int. J. Mod. Phys. C **9**, 887 (1998).
[37] H. W. J. Blöte and Y. J. Deng, Cluster Monte Carlo simulation of the transverse Ising model, Phys. Rev. E **66**, 066110 (2002).
[38] Y. J. Deng and H. W. J. Blöte, Monte Carlo study of the site-percolation model in two and three dimensions, Phys. Rev. E **72**, 016126 (2005).
[39] E. M. Elci, M. Weigel, and N. G. Fytas, Bridges in the random-cluster model, Nucl. Phys. B **903**, 19 (2016).
[40] R. van der Hofstad and W. Kager, Pattern theorems, ratio limit theorems and Gumbel maximal clusters for random fields, J. Stat. Phys. **130(3)**, 503 (2008).
[41] T. Łuczak, B. Pittel, and J. C. Wierman, The structure of a random graph at the point of the phase transition, Trans. Amer. Math. Soc. **341**, 721 (1994).
[42] R. M. Ziff, S. R. Finch, and V. S. Adamchik, Universality of Finite-Size Corrections to the Number of Critical Percolation Clusters, Phys. Rev. Lett. **79**, 3447 (1997).
[43] H. Hu, R. M. Ziff, and Y. J. Deng, No-Enclave Percolation Corresponds to Holes in the Cluster Backbone, Phys. Rev. Lett. **117**, 185701 (2016).
[44] P. H. Lundow and K. Markström, Complete graph asymptotics for the Ising and random-cluster models on five-dimensional grids with a cyclic boundary, Phys. Rev. E **91**, 022112 (2015).